Femtosecond Time-Resolved Neighbor Roles in the Fragmentation Dynamics of Molecules in a Dimer

Xitao Yu,[1,2] Xinyu Zhang,[1,2] Xiaoqing Hu,[3] Xinning Zhao,[1,2] Dianxiang Ren,[1,2] Xiaokai Li,[1,2] Pan Ma,[1,2] Chuncheng Wang,[1,2] Yong Wu,[3] Sizuo Luo,[1,2,*] and Dajun Ding[1,2,†]

[1]*Institute of Atomic and Molecular Physics, Jilin University, Changchun 130012, China*

[2]*Jilin Provincial Key Laboratory of Applied Atomic and Molecular Spectroscopy, Jilin University, Changchun 130012, China*

[3]*Institute of Applied Physics and Computational Mathematics, Beijing 100088, China*

(Received 21 December 2021; revised 7 April 2022; accepted 26 May 2022; published 5 July 2022)

How the neighbor effect plays its role in the fragmentation of molecular clusters attracts great attention for physicists and chemists. Here, we study this effect in the fragmentation of N_2O dimer by performing three-body coincidence measurements on the femtosecond timescale. Rotations of bound N_2O^+ triggered by neutral or ionic neighbors are tracked. The forbidden dissociation path between $B^2\Pi$ and $^4\Pi$ is opened by the spin-exchange effect due to the existence of neighbor ions, leading to a new channel of $N_2O^+ \rightarrow NO + N^+$ originating from $B^2\Pi$. The formation and dissociation of the metastable product $N_3O_2^+$ from two ion-molecule reaction channels are tracked in real time, and the corresponding trajectories are captured. Our results demonstrate a significant and promising step towards the understanding of neighbor roles in the reactions within clusters.

DOI: 10.1103/PhysRevLett.129.023001

van der Waals interactions are ubiquitous in nature and important to many physical and chemical phenomena [1–4]. In contrast to isolated atoms and molecules, the surrounding molecules in molecular complexes can serve as environments by dissipating the transferred excitation energy among the available degrees of freedom in the system [5–7]. It is demonstrated that environmental effects are widely present in various physical and chemical processes. A prominent example is the interatomic Coulomb decay (ICD) [8,9], where an inner-valence hole state in a weakly bonded system can undergo ultrafast relaxation and lead to electron emission from neighboring sites by energy transfer. Research on the roaming mechanism of H_3 shows that the chemical environment inhibits its formation [10]. Ion irradiation of fullerenes or polycyclic aromatic hydrocarbon clusters can promote the formation of hydrocarbon compounds [11,12], which is an important process in biochemical reactions induced by the ion-molecule collision within clusters [13–15].

Recently, the dissociation mechanisms of molecular dimers have attracted great attention [16–27]. Among them, it is demonstrated that the neighbor ions in a dimer play an important role in molecular dissociation. The presence of N_2^+ in $(N_2)_2$ affects the molecular fragmentation and shifts the potential energy curves (PECs) of the dication [23]. The adjacent CO^+ breaks the symmetry of CO^{2+} states, which induces an avoided crossing and generates a new dissociation channel [24]. However, this channel has been assigned to the contribution of higher-lying excitation states that existed in the molecular dissociation [25]. The neighbor Ar cation in divalent N_2Ar changes the barrier width of the PECs, resulting in tunneling with heavy nucleus transfer [26]. Ultrafast rotation can be excited by a neighboring molecule in dimers [27]. However, tracking how the neighboring ions affect the molecular dissociation in the cluster, on a femtosecond (fs) timescale, remains quite unexplored, including the molecular rotational excitation, the forbidden dissociation channel opening, and ion-molecule collision in the dimer.

Here, we have tracked such neighbor roles on the fs timescale by performing a pump-probe study on the fragmentation dynamics of N_2O dimer in cold target recoil ion momentum spectroscopy (COLTRIMS) (see Supplemental Material (SM) [28] and our previous work [29–31]). With a three-body coincidence measurement, the dissociation channels $NO^+ + N$ and $NO + N^+$ from N_2O^+ are resolved and the effects of neutral and ionic neighbors on the molecular cation dissociation can be further compared. The dimer is produced by expanding 2 bar N_2O gas through a 30 μm nozzle. Then, it interacts with a linearly polarized pump laser (800 nm, ~40 fs, 1.0×10^{14} W/cm^2). The produced fragments are ionized by an elliptically polarized probe laser (3.5×10^{14} W/cm^2, ~40 fs, and $\varepsilon \sim 0.7$) and are then guided by an electrostatic field toward a time- and position-sensitive detector. As a result, the time-resolved three-body Coulomb explosion (CE) channel ($N^+ + NO^+ + N_2O^+$) is measured coincidentally.

Figure 1(a) shows the measured time-dependent kinetic energy release (KER) spectrum from a three-body CE

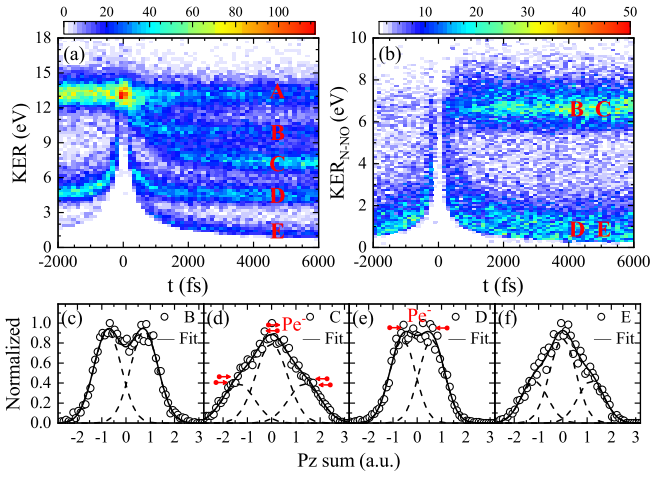

FIG. 1. (a) Time-dependent KER of three-body fragmentation channel of $(N_2O)_2$. (b) Time-dependent $KER_{N\text{-}NO}$ of the breakup of the N-NO bond for channels B, C, D, and E. (c)–(f) Corresponding ion sum-momentum distributions along the z axis (Pz_{sum}) for channels B to E.

channel, $(N_2O)_2^{3+} \rightarrow N^+ + NO^+ + N_2O^+$, wherein the spectrum is split into five branches (denoted as channel A, B, C, D, and E). As the pump-probe time delay increases, channel A has constant KER (~13 eV) which comes from the direct CE of $(N_2O)_2^{3+}$ produced by one of the pulses. The KERs of channels B–E decrease gradually as a function of time to the asymptotic energies, 10.0, 7.3, 4.5, and 1.2 eV at 6000 fs. These four branches correspond to pump-induced dissociation of the dimer.

To interpret the neighbor effects during the inter- and intramolecular fragmentation, we first need to identify the charge states and dissociation pathways of these four channels. For each channel, the charge states of the parent ion are prepared by the pump pulse and measured by the channel-resolved Pz_{sum} as shown in Figs. 1(c)–1(f), where $Pz_{sum} = Pz_{NO^+} + Pz_{N^+} + Pz_{N_2O^+} = Pz_{e1} + Pz_{e2} + Pz_{e3}$. Because the momentum of electrons released from the linearly polarized pump laser mainly distributes along the polarization direction (y axis) [32,33], and the one released from the elliptically polarized probe laser mainly contributes along the minor polarization axis (z axis) [34–36], the peak structure of the Pz_{sum} provides a clue for the number of electrons ionized from the elliptically polarized laser [29,37]. The double-peak and three-peak structures show one and two electrons are released from the probe laser [37], as shown in Figs. 1(c)–1(f). Consequently, this indicates that channels C and E are generated from the dissociation of $(N_2O)_2^+$, while channels B and D come from $(N_2O)_2^{2+}$.

The sequence of the breakup of the intermolecular (N_2O-N_2O) and intramolecular bond (N-NO) for these channels can be determined by measuring the time-dependent KER of N-NO, $KER_{N\text{-}NO}$ (see SM [28,38]), as is shown in Fig. 1(b) where the total KER is chosen between 0 and 11.5 eV. The diagram splits into two parts, where the part corresponding to channels B and C shows time-independent characteristics, indicating that there is no stretching of the intramolecular bond after the pump pulse, while the time-dependent part from the channels D and E indicates that the N-NO bond is breaking. Together with the identified charge states mentioned above, the pathways for channels B to E can be expressed as

$$B: (N_2O)_2 \xrightarrow{mh\nu} (N_2O)_2^{2+} + 2e^- \rightarrow N_2O^+ + N_2O^+ + 2e^-,$$

$$C: (N_2O)_2 \xrightarrow{nh\nu} (N_2O)_2^{+} + e^- \rightarrow N_2O^+ + N_2O + e^-,$$

$$D: (N_2O)_2 \xrightarrow{mh\nu} (N_2O)_2^{2+} + 2e^- \rightarrow N_2O^+ + NO^{p+} + N^{(1-p)+} + 2e^-,$$

$$E: (N_2O)_2 \xrightarrow{nh\nu} (N_2O)_2^{+} + e^- \rightarrow N_2O + NO^+ + N + e^-,$$

where $p = 1$, 0 for D_L and D_R channels as mentioned below. After dissociation, the fragments are further ionized by the probe laser and lead to three ions N_2O^+, NO^+, and N^+.

Based on the assignments, the effects of charged or neutral neighbors on bound and dissociating N_2O^+ can be studied separately. Three interesting phenomena during fragmentation induced by the neighbors are studied: molecular rotation, the opening of the forbidden dissociation channel, and ion-molecule collision in the dimer.

First, we focus on how the neighbors influence the bound N_2O^+ to visualize molecular rotation in channels B and C. Their rotational dynamics can be determined by the corresponding Newton diagrams, as shown in Figs. 2(a) and 2(b) (see SM [28] for the time-resolved Newton diagrams). For channel B, the Newton diagram shows a nearly isotropic distribution, which indicates the existence of rotational excitations of the intermediate N_2O^+ [24,38,39]. Channel C shows a concentrated distribution similar to the Newton diagrams of concerted fragmentation [39], indicating that less rotational excitation of N_2O occurs in this channel.

The rotation of the molecules can be manifested as the angle between the dissociation directions of inter- and intramolecular bonds, i.e., θ_{12} for channels B and C, as shown in Figs. 2(c) and 2(d). The width of θ_{12} for both channels becomes broader when the time delay is increased, indicating that the rotation of N_2O^{2+} occurs during the intermolecular bond breakup. Notably, the distribution of θ_{12} for channel B is wider than that of channel C at the same delay, proving that the rotation of N_2O^+ also depends on the charge state of the departing neighbor molecules. In the quantum view, the rotational excitation can occur during the half-collision process of dissociation [40,41], and the rotation of molecules is accumulated from the total contribution of repulsion during bond breaking. In channel B, the repulsion between the two N_2O^+ ions is stronger, while in channel C, the repulsion between N_2O^+ and N_2O is weaker. Therefore, the width of θ_{12} distribution is narrower at the same delay time. Moreover, we simulated the rotational dynamics of

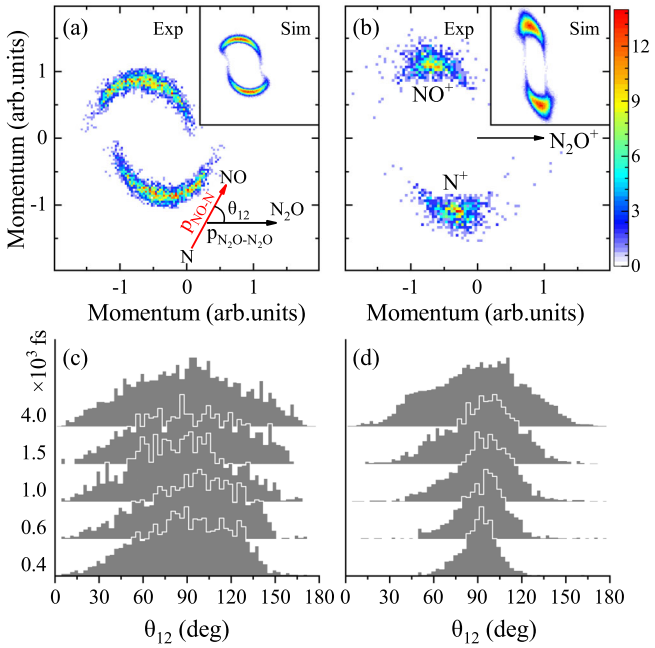

FIG. 2. Newton diagrams of channels (a) B and (b) C at 400 fs, where the momenta of fragments are normalized according to N_2O^+ which defines the x axis; and that of the NO^+ defines the positive side of the y axis, the inserted Newton diagrams are from simulations. Time-resolved distributions of θ_{12} for channels B (c) and C (d), where the definition of θ_{12} is shown in (a).

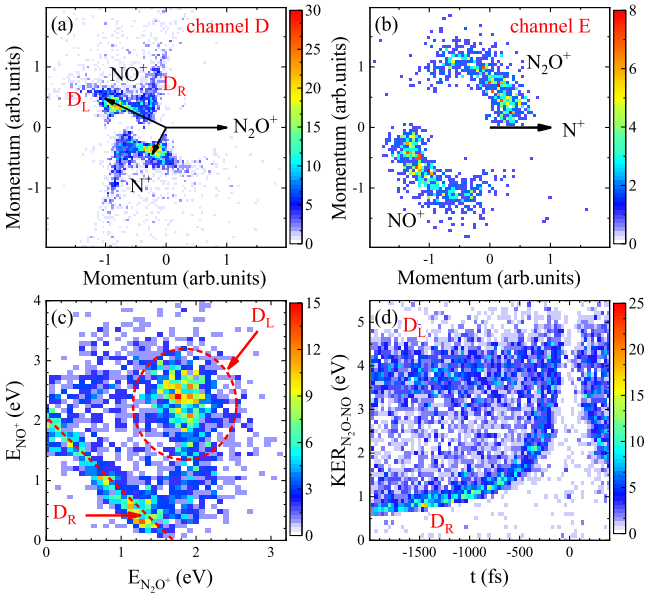

FIG. 3. Newton diagrams of channels (a) D and (b) E at 1000 fs, where the momenta of fragments are normalized according to N_2O^+ and N^+, respectively, and the definitions of coordinates are shown as arrows. (c) Kinetic energy correlation of N_2O^+ and NO^+ for channel D at 1000 fs. (d) Time-dependent $KER_{N_2O\text{-}NO}$ of channel D, where $KER_{N_2O\text{-}NO}$ is the KER of the breakup of the $(N_2O \cdot NO)^{2+}$ in native frames.

channels B and C (see SM [28]), showing good agreement with the experimental results. The observations demonstrate that the influence of a neutral and singly charged N_2O neighbor molecule on the ultrafast rotation of molecular ions can be observed by time-resolved CE imaging measurements.

The other neighbor effects on dissociative N_2O^+ are observed in the dissociation process of channels D and E, which can be preliminarily determined by their Newton diagrams, as shown in Figs. 3(a) and 3(b). There are two subsets marked as D_L and D_R for channel D, while only one subset is observed for channel E. Figure 3(c) gives the correlation map of the kinetic energy of NO^+ and N_2O^+ for channel D. The fixed energy correlation in the D_L channel indicates that these two ions are generated simultaneously, i.e., the $(N_2O)_2{}^{2+}$ directly breaks into three fragments. In Fig. 3(a), the arrow lengths represent the relative momenta of the fragments. N^+ has the smallest momentum, which means a neutral N atom is produced from the first dissociation step, i.e., the dissociation can be expressed as follows: D_L: $(N_2O)_2{}^{2+} \rightarrow NO^+ + N + N_2O^+$.

For the D_R channel, the distribution along the red-dashed line in Fig. 3(c) shows a total kinetic energy sharing between NO^+ and N_2O^+. It indicates that an intermediate product, $N_3O_2{}^+$, which has been observed in VUV photoionization of a N_2O dimer [42], is generated during the fragmentation process [22,30]. This identification is further confirmed by a simulation of kinetic energy correlation maps of the fragments (see SM [28]). However, the formation and dissociation of this product remains unexplored. Here, we can distinguish them by the time-dependent KER spectrum of $(N_2O \cdots NO)^{2+}$, i.e., $KER_{N_2O\text{-}NO}$, as shown in Fig. 3(d), where the time delay is negative, i.e., probe before pump, and the KER is limited to be 0–11.5 eV. In the negative time delay, the signal mainly comes from the D channel, as shown in Fig. 1(a). The branch from channel D_R shows that the $KER_{N_2O\text{-}NO}$ decreases with the time delay (also seen in SM [28] for time-resolved correlation maps of $KER_{N_2O\text{-}NO}$ and θ_{12}). This indicates that $N_3O_2{}^+$ is dissociating before the probe pulse arrives, and can be expressed as D_R: $(N_2O)_2{}^{2+} \rightarrow NO \cdots N_2O^+ + N^+ \rightarrow NO + N_2O^+ + N^+$.

Similarly, the kinetic energies of NO^+ and N_2O^+ for channel E share a total energy and the Newton diagram for channel E in Fig. 3(b) shows circular distributions, indicating the formation of intermediates $N_2O \cdots NO^+$ or $N_2O \cdots NO$ occurs. The charge should be assigned to NO after the first dissociation process since the momentum of NO^+ is larger than N^+ (see SM [28]). Furthermore, the binding energy of $N_2O \cdots NO$ (0.04 eV) [43] is much lower than the kinetic energy of NO (0.4 eV at 6 ps), hence it is impossible to form $N_2O \cdots NO$. Thus, the intermediates are $N_2O \cdots NO^+$ and channel E can be expressed as, $(N_2O)_2{}^+ \rightarrow N_2O \cdots NO^+ + N \rightarrow NO^+ + N_2O + N$, where N_2O^+ dissociates through $N_2O^+ \rightarrow NO^+ + N$.

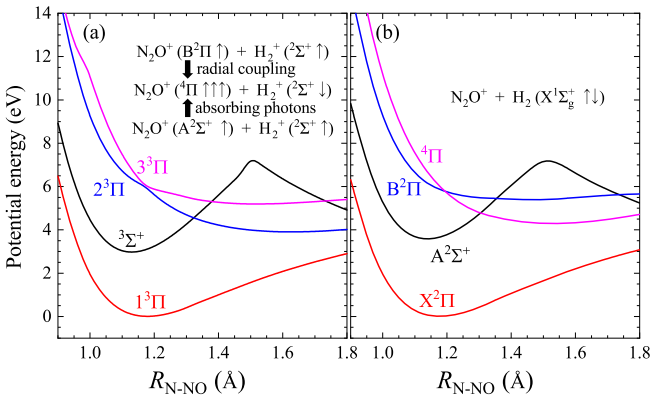

FIG. 4. (a) and (b) are *ab initio* PECs of the $N_2O^+ - H_2^+$ and $N_2O^+ - H_2$ complex. The spin flip of H_2^+ changes all the doublet states and the quadruplet state to triplet states. The intermolecular distance is set to 10 a.u. in the calculation.

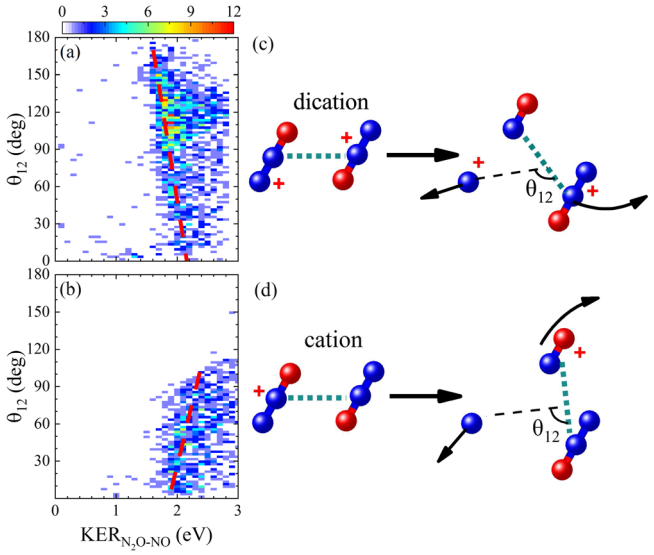

FIG. 5. Diagrams of $KER_{N_2O\text{-}NO}$ versus θ_{12} for analogous sequential channels (a) D_R and (b) E at 400 fs. The schematics of the fragmentation process of (c) D_R and (d) E.

These identifications indicate that the dissociation pathways of N_2O^+ differ greatly when neighboring with a neutral (channel E) or ionic (channel D) molecule. In channel D, the dissociation occurs through two pathways $NO^+ + N$ (D_L) and $NO + N^+$ (D_R), (the yield ratio N^+/NO^+ is about 0.6) while only $NO^+ + N$ appears in the channel E. The product of $NO^+ + N$ can be generated both from $B^2\Pi$ (lifetime ~30 fs) and $C^2\Sigma^+$ (~2000 fs) states during molecular dissociation in the fs-ps timescale [44–49], while the population of the $B^2\Pi$ state is much higher than the $C^2\Sigma^+$ state because of the rate of strong-field ionization [30]. The fast evolution of KER observed in channel D also indicates that the dissociation occurs from the $B^2\Pi$ state. In a monomer, the dissociation of the $B^2\Pi$ state ends to $NO^+ + N$ or $N_2^+ + O$ [47–50], while the ratio N^+/NO^+ from $B^2\Pi$ is approximately zero because the $NO + N^+$ is the product of $^4\Pi$ state [47–49] and the transition between other states ($A^2\Sigma^+$, $B^2\Pi$, and $C^2\Sigma^+$) and $^4\Pi$ states is forbidden. The coupling between the $^4\Pi$ and $C^2\Sigma^+$ state due to spin-orbit interaction can induce transitions, however, the yield ratio of N^+/NO^+ is less than 0.26 in molecules [44,51].

To interpret the observation of channel D_R, $(N_2O)_2^{2+} \rightarrow NO\cdots N_2O^+ + N^+$, we calculated the related PECs of N_2O^+ by the complete active space self-consistent field (CASSCF) method [52,53]. The results are given in Fig. 4, where the neighbor N_2O^+/N_2O is replaced by H_2^+/H_2. Comparing these two PECs, an obvious difference can be found, which comes from the spin-exchange between N_2O and H_2. Under the influence of H_2^+, all the doublet states ($X^2\Pi$, $A^2\Sigma^+$, and $B^2\Pi$) and the quadruplet state ($^4\Pi$) are changed to triplet states as shown in Fig. 4(a). However, the PECs of N_2O^+ neighboring to H_2 are the same as the ones of a monomer, which indicates that the neutral H_2 does not affect the breakup of N_2O^+. As a result, an avoided intersection can be formed between $2^3\Pi$ and $3^3\Pi$ which proves that the doublet $B^2\Pi$ is able to transition to the quadruplet $^4\Pi$ with a spin flip from the neighboring H_2^+. Similarly, the $^3\Sigma^+$ formed by $A^2\Sigma^+$ and H_2^+ can also transition to the $2^3\Pi/3^3\Pi$ and dissociate to NO and N^+ by absorbing photons. The spin-exchange effect is expected to be stronger when the neighbor is N_2O^+, while in the case of a neutral neighbor N_2O, the parity of states remains the same as a monomer, which explains why the observation of channel E only has $NO^+ + N$ products.

Moreover, both D_R and E channels have metastable intermediates ($NO\cdots N_2O^+$ or $N_2O\cdots NO^+$). To clarify their formation and dissociation dynamics, we plot the correlation maps of their KERs and the angle between the directions of the two-step dissociation, θ_{12}, as shown in Figs. 5(a) and 5(b). θ_{12} increases for channel D_R and decreases for channel E when the $KER_{N_2O\text{-}NO}$ decreases. Note that, since the $KER_{N_2O\text{-}NO}$ decreases as time increases, we can conclude that the θ_{12} decreases in channel E and increases in channel D_R as the delay increases. The decreasing θ_{12} in channel E indicates that the NO^+ flies away from N and is captured by N_2O as shown in Fig. 5(d). Furthermore, this is also confirmed by the time-resolved measurements, where the $KER_{N_2O\text{-}NO}$ decreases and θ_{12} localizes to a smaller angle as the delay time increases (see SM [28]). The dissociation schematic is shown in Fig. 5(d), where the dissociation of the N_2O^+ gives an initial velocity to NO^+ and the attraction from N_2O leads to the rotation of NO^+ around N_2O. Nevertheless, the N_2O fails to capture NO^+ because the kinetic energy of NO^+ from $B^2\Pi$ (~0.4 eV at 6 *ps* in our experiment) is higher than the binding energy of $N_2O\cdots NO^+$ (0.2–0.3 eV) [42,54], thus, two fragments flying away from each other. A similar dissociation occurs in channel D_R as shown in Figs. 5(a)

and 5(c). The different dependence as marked in the dashed lines in channel E and D_R shows the rotation of the $N_2O\cdots NO^+$ is opposite to the channel E. Because the repelling energy between N^+ and N_2O^+ is higher than that from the dissociation of N_2O^+ molecules, θ_{12} increases gradually as time increases as shown in Figs. 5(a) and 5(c), this is also confirmed by the simulations and time-dependent measurements (see SM [28]). These observations demonstrate that the neighbors can interact with the fragments generated from molecular dissociation.

In conclusion, we have tracked the neighbor effects on the fragmentation of a dimer in fs time-resolved CE imaging. When using a neighbor molecule as a reference, the ultrafast rotation of stable N_2O^+ induced by the neighbors is imaged. A fast rotation of N_2O^+ is observed when the neighbor is a molecular ion and the rotation is slower when the neighbor is a neutral molecule. The existence of a neighbor ion changes the yield ratio of products by modifying the parity of states during molecular dissociation because of the spin-exchange effect. After the dissociation, the neighbor also interacts with the produced fragments in the dimer, both N_2O with NO^+, and N_2O^+ with NO, which leads to the metastable product $N_3O_2^+$. The formation and dissociation dynamics of these products have been captured on the fs timescale. These observations contribute a significant step to understanding of how the neighbor effect influences the fragmentation of molecular clusters, DNA, and proteins, which also will have a strong impact on controlling chemical reactions since the reactivity strongly depends on the relative orientation and the charge state of molecules and its neighbors.

This work was supported by the National Basic Research Program of China (Grant No. 2019YFA0307700), the National Natural Science Foundation of China (Grants No. 12074143, No. 12134005, and No. 11627807), the Fundamental Research Funds for the Central Universities.

*luosz@jlu.edu.cn
†dajund@jlu.edu.cn

[1] L. Turi, W.-S. Sheu, and P. J. Rossky, Characterization of excess electrons in water-cluster anions by quantum simulations, Science **309**, 914 (2005).
[2] R. N. Pribble and T. S. Zwier, Size-specific infrared spectra of benzene-$(H_2O)_n$ clusters ($n = 1$ through 7): Evidence for noncyclic $(H_2O)_n$ structures, Science **265**, 75 (1994).
[3] T. Fennel, K.-H. Meiwes-Broer, J. Tiggesbäumker, P.-G. Reinhard, P. M. Dinh, and E. Suraud, Laser-driven nonlinear cluster dynamics, Rev. Mod. Phys. **82**, 1793 (2010).
[4] D. A. Dougherty, The cation-π interaction, Acc. Chem. Res. **46**, 885 (2013).
[5] X. Ren, E. Wang, A. D. Skitnevskaya, A. B. Trofimov, K. Gokhberg, and A. Dorn, Experimental evidence for ultrafast intermolecular relaxation processes in hydrated biomolecules, Nat. Phys. **14**, 1062 (2018).
[6] X. Ren, J. Zhou, E. Wang, T. Yang, Z. Xu, N. Sisourat, T. Pfeifer, and A. Dorn, Ultrafast energy transfer between π-stacked aromatic rings upon inner-valence ionization, Nat. Chem. **14**, 232 (2022).
[7] E. Wang, X. Ren, W. Baek, H. Rabus, T. Pfeifer, and A. Dorn, Water acting as a catalyst for electron-driven molecular break-up of tetrahydrofuran, Nat. Commun. **11**, 2194 (2020).
[8] L. S. Cederbaum, J. Zobeley, and F. Tarantelli, Giant Intermolecular Decay and Fragmentation of Clusters, Phys. Rev. Lett. **79**, 4778 (1997).
[9] S. Marburger, O. Kugeler, U. Hergenhahn, and T. Möller, Experimental Evidence for Interatomic Coulombic Decay in Ne Clusters, Phys. Rev. Lett. **90**, 203401 (2003).
[10] E. Wang, X. Ren, and A. Dorn, Role of the Environment in Quenching the Production of H_3^+ from Dicationic Clusters of Methanol, Phys. Rev. Lett. **126**, 103402 (2021).
[11] H. Zettergren *et al.*, Formations of Dumbbell C_{118} and C_{119} Inside Clusters of C_{60} Molecules by Collision with α Particles, Phys. Rev. Lett. **110**, 185501 (2013).
[12] R. Delaunay, M. Gatchell, P. Rousseau, A. Domaracka, S. Maclot, Y. Wang, M. H. Stockett, T. Chen, L. Adoui, M. Alcamí, F. Martín, H. Zettergren, H. Cederquist, and B. A. Huber, Molecular growth inside of polycyclic aromatic hydrocarbon clusters induced by ion collisions, J. Phys. Chem. Lett. **6**, 1536 (2015).
[13] T. A. Steitz and J. A. Steitz, A general two-metal-ion mechanism for catalytic RNA, Proc. Natl. Acad. Sci. U.S.A. **90**, 6498 (1993).
[14] P. Douzou and P. Maurel, Ionic control of biochemical reactions, Trends Biochem. Sci. **2**, 14 (1977).
[15] B. Brutschy, Ion-molecule reactions within molecular clusters, Chem. Rev. **92**, 1567 (1992).
[16] J. Voigtsberger *et al.*, Imaging the structure of the trimer systems $^4He_3$ and $^3He^4He_2$, Nat. Commun. **5**, 5765 (2014).
[17] J. Wu, M. Kunitski, L. P. H. Schmidt, T. Jahnke, and R. Dörner, Structures of N_2Ar, O_2Ar, and O_2Xe dimers studied by Coulomb explosion imaging, J. Chem. Phys. **137**, 104308 (2012).
[18] A. Khan, T. Jahnke, S. Zeller, F. Trinter, M. Schöffler, L. P. H. Schmidt, R. Dörner, and M. Kunitski, Visualizing the geometry of hydrogen dimers, J. Phys. Chem. Lett. **11**, 2457 (2020).
[19] J. D. Pickering, B. Shepperson, B. A. K. Hübschmann, F. Thorning, and H. Stapelfeldt, Alignment and Imaging of the CS_2 Dimer Inside Helium Nanodroplets, Phys. Rev. Lett. **120**, 113202 (2018).
[20] J. D. Pickering, B. Shepperson, L. Christiansen, and H. Stapelfeldt, Femtosecond laser induced Coulomb explosion imaging of aligned OCS oligomers inside helium nanodroplets, J. Chem. Phys. **149**, 154306 (2018).
[21] B. Ulrich, A. Vredenborg, A. Malakzadeh, L. P. H. Schmidt, T. Havermeier, M. Meckel, K. Cole, M. Smolarski, Z. Chang, T. Jahnke, and R. Dörner, Imaging of the structure of the argon and neon dimer, trimer, and tetramer, J. Phys. Chem. A **115**, 6936 (2011).
[22] X. Yu, X. Zhao, Z. Wang, Y. Yang, X. Zhang, P. Ma, X. Li, C. Wang, X. Xu, C. Wang, D. Zhang, S. Luo, and D. Ding, Determining the stereo configuration of carbonyl sulfide

dimers using Coulomb-explosion imaging, Phys. Rev. A **104**, 053104 (2021).

[23] A. Méry, A. N. Agnihotri, J. Douady, X. Fléchard, B. Gervais, S. Guillous, W. Iskandar, E. Jacquet, J. Matsumoto, J. Rangama, F. Ropars, C. P. Safvan, H. Shiromaru, D. Zanuttini, and A. Cassimi, Role of a Neighbor Ion in the Fragmentation Dynamics of Covalent Molecules, Phys. Rev. Lett. **118**, 233402 (2017).

[24] X. Ding, M. Haertelt, S. Schlauderer, M. S. Schuurman, A. Y. Naumov, D. M. Villeneuve, A. R. W. McKellar, P. B. Corkum, and A. Staudte, Ultrafast Dissociation of Metastable CO^{2+} in a Dimer, Phys. Rev. Lett. **118**, 153001 (2017).

[25] A. Méry, V. Kumar, X. Fléchard, B. Gervais, S. Guillous, M. Lalande, J. Rangama, W. Wolff, and A. Cassimi, Coulomb-explosion imaging of carbon monoxide dimers, Phys. Rev. A **103**, 042813 (2021).

[26] X. Zhu, X. Hu, S. Yan, Y. Peng, W. Feng, D. Guo, Y. Gao, S. Zhang, A. Cassimi, J. Xu, D. Zhao, D. Dong, B. Hai, Y. Wu, J. Wang, and X. Ma, Heavy N^+ ion transfer in doubly charged N_2Ar van der Waals cluster, Nat. Commun. **11**, 2987 (2020).

[27] J. Zhou, C. He, M.-M. Liu, E. Wang, S. Jia, A. Dorn, X. Ren, and Y. Liu, Real-time observation of ultrafast molecular rotation in weakly bound dimers, Phys. Rev. Research **3**, 023050 (2021).

[28] See Supplemental Material at http://link.aps.org/supplemental/10.1103/PhysRevLett.129.023001 for experimental setup, momentum and KER calculation in the sequential fragmentation in native frames, time-resolved Newton diagrams and correlation maps of angle and KER in native frames for channels B to E, simulation of three-body sequential fragmentation, and the simulated and measured correlation maps of channel D_L.

[29] S. Luo, J. Liu, X. Li, D. Zhang, X. Yu, D. Ren, M. Li, Y. Yang, Z. Wang, P. Ma, C. Wang, J. Zhao, Z. Zhao, and D. Ding, Revealing Molecular Strong Field Autoionization Dynamics, Phys. Rev. Lett. **126**, 103202 (2021).

[30] X. Zhao, X. Yu, X. Xu, Z. Yin, J. Yu, X. Li, P. Ma, D. Zhang, C. Wang, S. Luo, and D. Ding, Ultrafast dissociation dynamics of singly and doubly ionized N_2O in strong laser fields, Phys. Rev. A **101**, 013416 (2020).

[31] X. Zhao, T. Xu, X. Yu, D. Ren, X. Zhang, X. Li, P. Ma, C. Wang, D. Zhang, Q. Wang, X. Hu, S. Luo, Y. Wu, J. Wang, and D. Ding, Tracking the nuclear movement of the carbonyl sulfide cation after strong-field ionization by time-resolved Coulomb-explosion imaging, Phys. Rev. A **103**, 053103 (2021).

[32] D. Comtois, D. Zeidler, H. Pépin, J. C. Kieffer, D. M. Villeneuve, and P. B. Corkum, Observation of Coulomb focusing in tunnelling ionization of noble gases, J. Phys. B **38**, 1923 (2005).

[33] A. Rudenko, K. Zrost, T. Ergler, A. B. Voitkiv, B. Najjari, V. L. B. de Jesus, B. Feuerstein, C. D. Schröter, R. Moshammer, and J. Ullrich, Coulomb singularity in the transverse momentum distribution for strong-field single ionization, J. Phys. B **38**, L191 (2005).

[34] P. Eckle, M. Smolarski, P. Schlup, J. Biegert, A. Staudte, M. Schöffler, H. G. Muller, R. Dörner, and U. Keller, Attosecond angular streaking, Nat. Phys. **4**, 565 (2008).

[35] A. N. Pfeiffer, C. Cirelli, M. Smolarski, R. Dörner, and U. Keller, Timing the release in sequential double ionization, Nat. Phys. **7**, 428 (2011).

[36] J. Wu, M. Meckel, L. Schmidt, M. Kunitski, S. Voss, H. Sann, H. Kim, T. Jahnke, A. Czasch, and R. Dörner, Probing the tunnelling site of electrons in strong field enhanced ionization of molecules, Nat. Commun. **3**, 1113 (2012).

[37] J. Wu, L. P. H. Schmidt, M. Kunitski, M. Meckel, S. Voss, H. Sann, H. Kim, T. Jahnke, A. Czasch, and R. Dörner, Multiorbital Tunneling Ionization of the CO Molecule, Phys. Rev. Lett. **108**, 183001 (2012).

[38] J. Rajput, T. Severt, B. Berry, B. Jochim, P. Feizollah, B. Kaderiya, M. Zohrabi, U. Ablikim, F. Ziaee, P. Kanaka Raju, D. Rolles, A. Rudenko, K. D. Carnes, B. D. Esry, and I. Ben-Itzhak, Native Frames: Disentangling Sequential from Concerted Three-Body Fragmentation, Phys. Rev. Lett. **120**, 103001 (2018).

[39] C. Wu, C. Wu, D. Song, H. Su, Y. Yang, Z. Wu, X. Liu, H. Liu, M. Li, Y. Deng, Y. Liu, L.-Y. Peng, H. Jiang, and Q. Gong, Nonsequential and Sequential Fragmentation of CO_2^{3+} in Intense Laser Fields, Phys. Rev. Lett. **110**, 103601 (2013).

[40] Y. B. Band, K. F. Freed, and D. J. Kouri, Half-collision description of final state distributions of the photodissociation of polyatomic molecules, J. Chem. Phys. **74**, 4380 (1981).

[41] K. T. Lorenz, D. W. Chandler, J. W. Barr, W. Chen, G. L. Barnes, and J. I. Cline, Direct measurement of the preferred sense of no rotation after collision with argon, Science **293**, 2063 (2001).

[42] S. H. Linn and C. Y. Ng, Photoionization study of CO_2, N_2O dimers and clusters, J. Chem. Phys. **75**, 4921 (1981).

[43] Z. Liu, X. Li, M. Ge, R. Zheng, and C. Duan, Structural characterization of the $NO(X^2\Pi) - N_2O$ complex with mid-infrared laser absorption spectroscopy and quantum chemical calculations, J. Chem. Phys. **152**, 154303 (2020).

[44] X. Tang, M. Niu, X. Zhou, S. Liu, F. Liu, X. Shan, and L. Sheng, NO^+ formation pathways in dissociation of N_2O^+ ions at the $C^2\Sigma^+$ state revealed from threshold photoelectron–photoion coincidence velocity imaging, J. Chem. Phys. **134**, 054312 (2011).

[45] M. Lebech, J. C. Houver, D. Dowek, and R. R. Lucchese, Dissociative photoionization of N_2O in the region of the $N_2O^+(C^2\Sigma^+)$ state, studied by ion-electron velocity vector correlation, J. Chem. Phys. **117**, 9248 (2002).

[46] H. Wang, X. Zhou, S. Liu, B. Jiang, D. Dai, and X. Yang, Predissociation dynamics of N_2O^+ at the $A^2\Sigma^+$ state: Three pathways to form $NO^+(^1\Sigma^+)$ revealed from ion velocity imaging, J. Chem. Phys. **132**, 244309 (2010).

[47] G. Chambaud, H. Gritli, P. Rosmus, H. J. Werner, and P. J. Knowles, The ion-molecule reaction $O^+(^4S) + N_2(X^1\Sigma^+) \rightarrow NO^+(X^1\Sigma^+; v') + N(^4S)$ and the predissociation of the $A^2\Sigma^+$ and $B^2\Pi$ states of N_2O^+, Mol. Phys. **98**, 1793 (2000).

[48] I. Nenner, P. Guyon, T. Baer, and T. R. Govers, A threshold photoelectron–photoion coincidence study of the N_2O^+ dissociation between 15 and 20.5 eV, J. Chem. Phys. **72**, 6587 (1980).

[49] M. Lebech, J. C. Houver, D. Dowek, and R. R. Lucchese, Dissociative photoionization of N_2O in the region of the $N_2O^+(B^2\Pi)$ state studied by ion–electron velocity vector correlation, J. Chem. Phys. **120**, 8226 (2004).

[50] P. O. Danis, T. Wyttenbach, and J. P. Maier, Two-photon absorption spectroscopy of mass-selected ions: N_2O^+ and CS_{2+}, J. Chem. Phys. **88**, 3451 (1988).

[51] E. Kinmond, J. Eland, and L. Karlsson, Dissociation of N_2O^+ ions from the valence states reached by one-photon photoionisation, Int. J. Mass Spectrom. **185–187**, 437 (1999).

[52] H.-J. Werner, P. J. Knowles, G. Knizia, F. R. Manby, and M. Schütz, Molpro: A general-purpose quantum chemistry program package, WIREs Comput. Mol. Sci. **2**, 242 (2012).

[53] H. J. Werner, P. J. Knowles, G. Knizia, F. R. Manby, M. Schütz, P. Celani, T. Korona, R. Lindh, A. Mitrushenkov, and G. Rauhut *et al.*, MOLPRO, a Package of *Ab Initio* Programs, Version 2010.1, http://www.molpro.net.

[54] A. J. Illies, Thermochemistry for the gas-phase ion-molecule clustering of $CO_2{}^+CO_2$, $SO_2{}^+CO_2$, $N_2O^+N_2O$, $O_2{}^+CO_2$, NO^+CO_2, $O_2{}^+N_2O$ and NO^+N_2O: Description of a new hybrid drift tube/ion source with coaxial electron beam and ion exit apertures, J. Phys. Chem. **92**, 2889 (1988).